Quantum anomalous Hall effect in twisted bilayer graphene quasicrystal*

Zedong Li(李泽东) and Z F Wang(王征飞)†

Hefei National Laboratory for Physical Sciences at the Microscale, CAS Key Laboratory of Strongly-Coupled Quantum Matter Physics, University of Science and Technology of China, Hefei 230026, China

(Received 6 May 2020; revised manuscript received 24 July 2020; accepted manuscript online 1 August 2020)

The nontrivial topology is investigated in a dodecagonal quasicrystal made of 30° twisted bilayer graphene (TBG). Based on tight-binding model with both exchange field and Rashba spin–orbit coupling, the topological index, chiral edge states, and quantum conductance are calculated to distinguish its unique topological phase. A high Bott index ($B = 4$) quantum anomalous Hall effect (QAHE) is identified in TBG quasicrystal, which is robust to a finite perturbation without closing the nontrivial gap. Most remarkably, we have found that the multiple Dirac cone replicas in TBG quasicrystal are only a spectra feature without generating extra chiral edge states. Our results not only propose a possible way to realize the QAHE in quasicrystal, but also identify the continuity of nontrivial topology in TBG between crystal and quasicrystal.

Keywords: quasicrystal, twisted bilayer graphene, quantum anomalous Hall effect

PACS: 71.23.Ft, 73.43.Cd, 72.15.Cz **DOI:** 10.1088/1674-1056/abab77

1. Introduction

Quantum anomalous Hall effect (QAHE), as a special class of topological phase, has been intensively studied in recent years.[1–4] Physically, it can be realized in a topological crystal with both spin–orbit coupling (SOC) and ferromagnetism. Although various two-dimensional (2D) crystal materials have been predicted theoretically to host QAHE,[5–14] only magnetic doped 2D topological insulator[15,16] and $MnBi_2Te_4$[17,18] are confirmed experimentally. Currently, it still remains a challenging task to realize the high-temperature QAHE in real crystal materials. In addition to these studies, the in-plane magnetization induced QAHE is also proposed,[19–22] demonstrating another way to search the candidate materials. However, all these prior works are limited in crystal materials, because the nontrivial topology is defined in the framework of Bloch band theory in periodic system. Recently, people found that the nontrivial topology can also be defined in non-periodic system, making it possible to study different kinds of topological phase in amorphous and quasicrystal materials.[23–30] This discovery greatly extends the scope of conventional topological materials, drawing great research interests.

Graphene, as the first experimentally confirmed 2D material, has opened a new research area since its discovery. Based on its Dirac band, a variety of topological phases have been predicted in this model system, such as quantum spin Hall,[31] topological valley Hall,[32] and QAHE.[7] Different Hamiltonian terms are studied in this system for creating exotic quantum phenomena, from the single-body to many-body physics.[33,34] Recently, the correlated state and superconductivity in twisted bilayer graphene (TBG)[35,36] become a hot research topic in condensed matter physics, bringing a new light to the field of high temperature superconductivity. TBG is constructed by two monolayers of graphene with a relative rotation between two layers,[37] exhibiting a new degree of freedom to manipulate its electronic structures. Most significantly, if the twist angle is $\theta = 30°$, TBG will be a quasicrystal with 12-fold rotational symmetry, showing a natural quasicrystal made of single carbon element.[38,39] The low-energy band of TBG quasicrystal is a little different to its counterpart with commensurate twist angle, in which Umklapp scattering induced multiple Dirac cone replicas are found in angle resolved photoemission spectra.[38]

In this work, based on tight-binding (TB) model calculations with both exchange field and Rashba SOC, the QAHE in TBG quasicrystal is studied. Firstly, a non-vanishing topological Bott index ($B = 4$) is found in our system, indicating four chiral edge states. Secondly, the bulk gap is extracted from the local density of state (LDOS) at lattice-site in the center region, then, the spatial distribution of chiral edge states within the bulk gap is investigated, showing the localized feature at the boundary. Due to the confinement, the continuous in-gap chiral edge states are discrete, whose number is linearly proportional to the system size. Thirdly, the quantum transport calculation is performed, and a quantized conductance of $G = 4e^2/h$ is obtained, which is robust to finite on-site and hopping disorders. These characterized features demonstrate a high Bott index QAHE in TBG quasicrystal. Physically,

*Project supported by the National Natural Science Foundation of China (Grant Nos. 11774325 and 21603210), the National Key Research and Development Program of China (Grant No. 2017YFA0204904), and Fundamental Research Funds for the Central Universities, China.

†Corresponding author. E-mail: zfwang15@ustc.edu.cn

our results also identify two extra points: (1) the exchange field and Rashba SOC have the similar effect in both crystal and quasicrystal, exhibiting a continuous topological phase in TBG; (2) the multiple Dirac cone replicas in TBG quasicrystal cannot generate extra chiral edge states, which is dramatically different to the conventional Dirac cone states. We believe these results will help people to better understand the nontrivial topology in TBG quasicrystal.

2. Methodology

Based on p_z orbital, the TB Hamiltonian of TBG quasicrystal can be written as[40]

$$H = H_{\rm u} + H_{\rm l} + H_{\rm int}, \tag{1}$$

$$H_{\rm u/l} = t_1 \sum_{\langle ij\rangle,\alpha} c^{\dagger}_{i\alpha} c_{j\alpha} + {\rm i}t_{\rm R} \sum_{\langle ij\rangle,\alpha\beta} (\boldsymbol{\sigma} \times \boldsymbol{d}_{ij})_z c^{\dagger}_{i\alpha} c_{j\beta} + \lambda \sum_{i,\alpha} c^{\dagger}_{i\alpha} c_{i\alpha} + {\rm h.c.}, \tag{2}$$

$$H_{\rm int} = t_2 \sum_{i\in{\rm up},\alpha} \sum_{j\in{\rm low},\alpha} c^{\dagger}_{i\alpha} c_{j\alpha} e^{-3(r_{ij}-3.35)} + {\rm h.c.}, \tag{3}$$

where $c^{\dagger}_{i\alpha}$ ($c_{i\alpha}$) is the creation (annihilation) operator at i-site with α-spin. Equation (2) is the intralayer Hamiltonian. The first-term is nearest-neighbor (NN) hopping, the second-term is Rashba SOC, and the third term is exchange field. t_1 is the NN hopping parameter, $t_{\rm R}$ is the intensity of Rashba SOC, $\boldsymbol{\sigma}$ is the Pauli matrix, $\boldsymbol{d}_{ij}$ is the vector connecting i-site and j-site, and λ is the intensity of exchange field. Equation (3) is the interlayer Hamiltonian. t_2 is the hopping parameter, r_{ij} is the distance between i-site on upper-layer and j-site on lower-layer. To maintain the 12-fold rotational symmetry, all interlayer hopping terms are considered.

Different to Penrose tiling quasicrystal with 5-fold rotational symmetry, it is hard to construct an approximate periodic boundary in TBG quasicrystal with 12-fold rotational symmetry. Therefore, we cannot directly obtain its bulk gap by imposing a periodic boundary condition as easy as previous works.[27,28] Alternatively, we use the local density of state (LDOS) to extract the bulk gap. To avoid the finite size effect, the LDOS at the center-lattice site is calculated by using millions of atoms with Lanczos recursive method.[41]

The Bott index is evaluated by a real-space method,[23,24,42–44] and the projector operator is defined as

$$P = \sum_{i=1}^{N_{\rm occ}} |\psi_i\rangle\langle\psi_i|, \tag{4}$$

where $|\psi_i\rangle$ is the i-th occupied state. The relevant projected position operators are

$$V_1 = P{\rm e}^{{\rm i}2\pi X}P, \quad V_2 = P{\rm e}^{{\rm i}2\pi Y}P, \tag{5}$$

where X and Y are the rescaled coordinates within the interval [0,1). Then, the Bott index can be calculated as

$$B = \frac{1}{2\pi}{\rm Im}\{{\rm Tr}[\log(VUV^{\dagger}U^{\dagger})]\}. \tag{6}$$

The conductance of chiral edge states in TBG quasicrystal is calculated by Landauer–Büttiker formula[45]

$$G = \frac{e^2}{h}{\rm Tr}[\Gamma_{\rm L} G^{\rm r}_{\rm c} \Gamma_{\rm R} G^{\rm a}_{\rm c}], \tag{7}$$

where $G^{\rm r}_{\rm c}$ and $G^{\rm a}_{\rm c}$ are the retarded and advanced Green's functions of center-scattering region. Γ matrix is defined as

$$\Gamma_{\rm L/R} = {\rm i}(\Sigma^{\rm r}_{\rm L/R} - \Sigma^{\rm a}_{\rm L/R}), \tag{8}$$

where $\Sigma^{\rm r}_{\rm L/R}$ and $\Sigma^{\rm a}_{\rm L/R}$ are the retarded and advanced self-energies of the left/right lead.

3. Results and discussion

Firstly, to identify the bulk topology of TBG quasicrystal with exchange field and Rashba SOC, its Bott index is calculated in a cluster configuration with open boundary condition, including over twelve-thousand atoms. For a constant exchange field and different values of Rashba SOC, the evaluated Bott index is shown in Fig. 1. One can see that $B = 4$ for all intensities of Rashba SOC, exhibiting a high Bott index QAHE. It is well known that the exchange field and Rashba SOC can induce a QAHE with $C = 2$ (Chern number) in monolayer graphene.[7] Since the Chern number in crystal is equivalent to the Bott index in quasicrystal, our results indicate that each graphene layer in TBG quasicrystal contributes a Bott index $B = 2$, corresponding to two chiral edge states. Therefore, the exchange field and Rashba SOC will have the same effect in both TBG crystal and quasicrystal, showing the continuity of QAHE. This conclusion is also supported by our Bott index calculations in TBG with a commensurate twist angle. Moreover, our results also indicate that the multiple Dirac cone replicas in TBG quasicrystal cannot generate extra Bott index or chiral edge states. Physically, they are induced by Umklapp scattering,[38] which are inequivalent to the Dirac cone states in conventional materials.

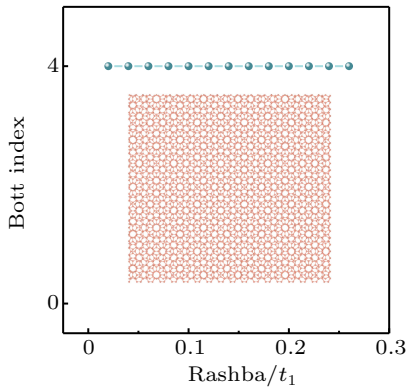

Fig. 1. Bott index of TBG quasicrystal with different intensities of $t_{\rm R}$. The inset is the atomic structure of TBG quasicrystal. $\lambda = 0.18t_1$ and $t_2 = 0.12t_1$.

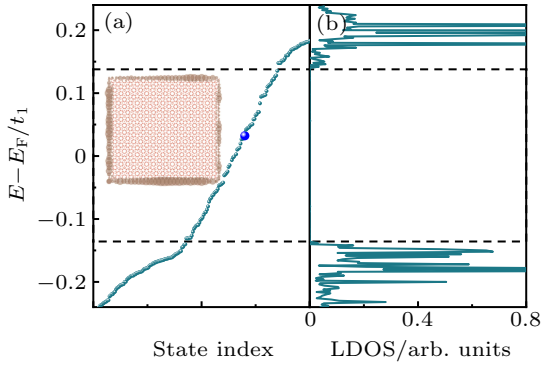

Fig. 2. (a) Discrete energy levels of TBG quasicrystal. (b) Bulk LDOS of TBG quasicrystal. The two dashed lines denote the region of bulk gap. The discrete energy levels in bulk gap are the in-gap chiral edge states. The spatial distribution of in-gap chiral edge state at the energy level marked by the blue dot is shown in the inset of (a), which is localized at the boundary of TBG quasicrystal. The circle size denotes the weight of chiral edge state. $\lambda = 0.18t_1$, $t_R = 0.2t_1$, $t_2 = 0.12t_1$.

Secondly, to identify the chiral edge states in TBG quasicrystal, the spatial distribution of them is studied. The discrete energy levels of TBG quasicrystal with exchange field and Rashba SOC are shown in Fig. 2(a). In order to distinguish the bulk and edge states in TBG quasicrystal, one must obtain its bulk gap. The bulk LDOS at center-lattice site is calculated, as shown in Fig. 2(b). Aligning Figs. 2(a) and 2(b) together, the bulk gap and in-gap chiral edge states of TBG quasicrystal can be seen clearly, as denoted by two dashed lines. Here, one should not confuse the number of in-gap chiral edge states with Bott index $B = 4$. Since the chiral edge state in a crystal material is momentum dependent, it connects the valence and conduction band continuously. However, in a cluster configuration, due to the confinement, the continuous chiral edge states will become a set of discrete energy levels. To directly see the boundary feature of these chiral edge states, the spatial distribution of one chiral edge state at the energy level marked by a blue dot is shown in the inset of Fig. 2(a). Obviously, the in-gap chiral edge state is localized on the edge of the cluster.

Moreover, we have found that the nontrivial bulk gap of TBG crystal is tunable by Rashba SOC, similar to the case in monolayer graphene.[7] With the increasing intensity of Rashba SOC, the bulk LDOS of TBG quasicrystal is shown in Fig. 3(a). One can see the gradually increased nontrivial bulk gap, as denoted by two dashed lines. Since the in-gap chiral edge states are confined by the finite system size, the number of discrete in-gap chiral edge states will increase as the size of the system increases, eventually approaching the bulk limit and forming a continuous edge state without discrete gaps. The system size vs. the number of in-gap edge state is shown in Fig. 3(b), showing a linear increasing behavior, which is consistent with our expectation.

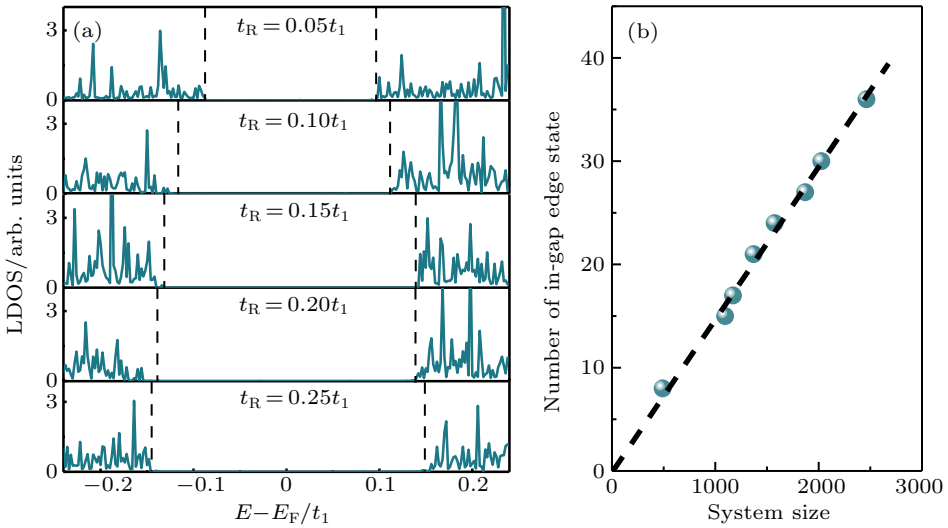

Fig. 3. (a) Bulk LDOS with different intensities of t_R. The two dashed lines denote the region of bulk gap. $\lambda = 0.18t_1$, $t_2 = 0.12t_1$. (b) The number of in-gap edge state vs. the system size. The dashed line is a linear fitting of the calculated results. $t_R = 0.2t_1$.

Lastly, to identify the robustness of these chiral edge states against disorder, the quantum transport calculations are performed. As shown in Fig. 4(a), a TBG quasicrystal ribbon with over four thousand atoms is constructed as the center-scattering region, which is connected to the left and right leads (described by a square lattice). Without disorder, the calculated conductance is shown in Fig. 4(b). A plateau region is observed around the Fermi level, which is comparable to the nontrivial bulk gap extracted from the LDOS. Here, the plateau is quantized to $G = 4e^2/h$, indicating four conducting channels on the edge. This is also consistent with the Bott index ($B = 4$) calculations. Furthermore, the LDOS distribution at the energy level inside and outside the plateau region, marked by the blue dots in Fig. 4(b), is shown in Figs. 4(c) and 4(d), respectively. Clearly, the LDOS in the plateau region is localized on the edge while the LDOS outside the plateau region is distributed uniformly in the bulk, showing the edge and bulk conducting channels, respectively. Since the chiral edge state in QAHE has a topological origin, which is robust to disorder induced backscattering if the nontrivial bulk

gap is not inverted. To check the robustness of QAHE, both on-site-energy disorder and hopping disorder are considered. In our calculations, a large number of disorder configurations have been considered, and the conductance is averaged among them. For the first type of disorder, a random on-site-energy with a uniform distribution within [-W, W] is added on the edge atoms. As shown in Fig. 4(e), a nearly quantized conductance of $G \sim 4e^2/h$ is observed around the Fermi level. For the second type of disorder, a random interlayer and intralayer bond-length-variation is added between edge atoms. As shown in Figs. 4(f) and 4(g), similar quantized conductance can be observed. Therefore, our proposed QAHE in TBG quasicrystal is very robust. In principle, the exchange field and Rashba SOC in TBG quasicrystal can be introduced by magnetic atom adsorption or magnetic substrate induced proximity effect, which have been intensively studied in previous works.[8,9,46]

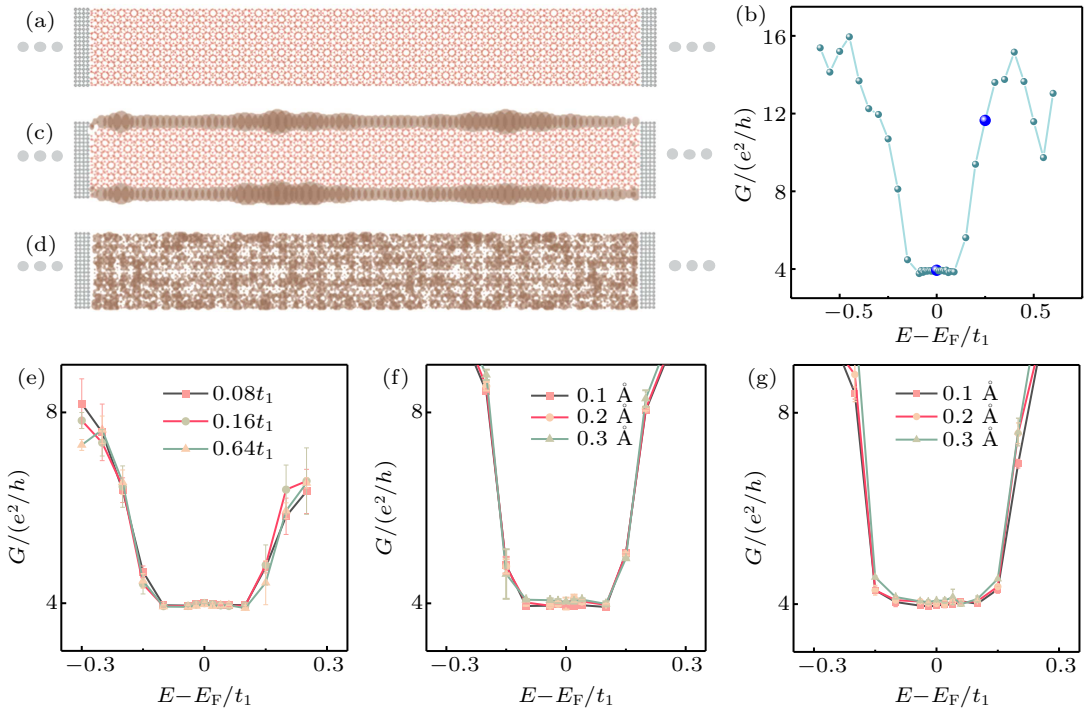

Fig. 4. (a) Device setup of the TBG quasicrystal ribbon. The square lattice denotes the semi-infinite lead region. (b) Conductance vs. the energy without disorder. (c) and (d) LDOS distribution in the center-scattering region at the energy level marked by the blue dots in (b). (e)–(g) Conductance vs. the energy with on-site-energy, interlayer, and intralayer hopping disorder, respectively. The error bar denotes the fluctuation of conductance among different disorder configurations. $\lambda = 0.18t_1, t_R = 0.2t_1, t_2 = 0.12t_1$.

4. Conclusion and perspectives

In summary, we propose a stable QAHE in TBG quasicrystal with a twist angle of 30°, which is identified by Bott index, chiral edge states, and quantized conductance calculations. Our results not only clarify the continuity of QAHE in TBG crystal and quasicrystal, but also confirm the multiple Dirac cone replicas in TBG quasicrystal to be a spectra feature, without any contribution to the chiral edge states in QAHE.

Acknowledgment

We thank Supercomputing Center at USTC for providing the computing resources.

References

[1] Haldane F D M 1988 *Phys. Rev. Lett.* **61** 2015
[2] He K, Wang Y and Xue Q K 2014 *Nat. Sci. Rev.* **1** 38
[3] Weng H, Yu R, Hu X, Dai X and Fang Z 2015 *Adv. Phys.* **64** 227
[4] Liu C X, Zhang S C and Qi X L 2016 *Annu. Rev. Condens. Matter Phys.* **7** 301
[5] Wang Z F, Liu Z and Liu F 2013 *Phys. Rev. Lett.* **110** 196801
[6] Yu R, Zhang W, Zhang H J, Zhang S C, Dai X and Fang Z 2010 *Science* **329** 61
[7] Qiao Z, Yang S A, Feng W, Tse W K, Ding J, Yao Y, Wang J and Niu Q 2010 *Phys. Rev. B* **82** 161414
[8] Ding J, Qiao Z, Feng W, Yao Y and Niu Q 2011 *Phys. Rev. B* **84** 195444
[9] Zhang H, Lazo C, Blügel S, Heinze S and Mokrousov Y 2012 *Phys. Rev. Lett.* **108** 056802
[10] Wang J, Lian B, Zhang H, Xu Y and Zhang S C 2013 *Phys. Rev. Lett.* **111** 136801
[11] Wu S C, Shan G and Yan B 2014 *Phys. Rev. Lett.* **113** 256401
[12] Dolui K, Ray S and Das T 2015 *Phys. Rev. B* **92** 205133
[13] Dong L, Kim Y, Er D, Rappe A M and Shenoy V B 2016 *Phys. Rev. Lett.* **116** 096601
[14] Wang Z F, Liu Z, Yang J and Liu F 2018 *Phys. Rev. Lett.* **120** 156406
[15] Chang C Z, Zhang J, Feng X, Shen J, Zhang Z, Guo M, Li K, Ou Y, Wei P, Wang L L, Ji Z Q, Feng Y, Ji S, Chen X, Jia J, Dai X, Fang Z, Zhang S C, He K, Wang Y, Lu L, Ma X C and Xue Q K 2013 *Science* **340** 167
[16] Bestwick A J, Fox E J, Kou X, Pan L, Wang K L and haber-Gordon D 2015 *Phys. Rev. Lett.* **114** 187201
[17] Deng Y, Yu Y, Shi M Z, Guo Z, Xu Z, Wang J, Chen X H and Zhang Y 2020 *Science* **367** 895
[18] Liu C, Wang Y, Li H, Wu Y, Li Y, Li J, He K, Xu Y, Zhang J and Wang Y 2020 *Nat. Mater.* **19** 522

[19] Liu X, Hsu H C and Liu C X 2013 *Phys. Rev. Lett.* **111** 086802
[20] Ren Y, Zeng J, Deng X, Yang F, Pan H and Qiao Z 2016 *Phys. Rev. B* **94** 085411
[21] Zhong P, Ren Y, Han Y, Zhang L and Qiao Z 2017 *Phys. Rev. B* **96** 241103(R)
[22] Liu Z, Zhao G, Liu B, Wang Z F, Yang J and Liu F 2018 *Phys. Rev. Lett.* **121** 246401
[23] Bandres M A, Rechtsman M C and Segev M 2016 *Phys. Rev. X* **6** 011016
[24] Agarwala A and Shenoy V B 2017 *Phys. Rev. Lett.* **118** 236402
[25] Liu C, Gao W, Yang B and Zhang S 2017 *Phys. Rev. Lett.* **119** 183901
[26] Mitchell N P, Nash L M, Hexner D, Turner A M and Irvine W T M 2018 *Nat. Phys.* **14** 380
[27] Huang H and Liu F 2018 *Phys. Rev. Lett.* **121** 126401
[28] Huang H and Liu F 2018 *Phys. Rev. B* **98** 12513
[29] Costa M, Schleder G R, Nardelli M B, Lewenkopf C and Fazzio A 2019 *Nano Lett.* **19** 8941
[30] Chen R, Chen C Z, Gao J H, Zhou Bin and Xu D H 2020 *Phys. Rev. Lett.* **124** 036803
[31] Kane C L and Mele E J 2005 *Phys. Rev. Lett.* **95** 226801
[32] Xiao D, Yao W and Niu Q 2007 *Phys. Rev. Lett.* **99** 236809
[33] Castro Neto A H, Guinea F, N Peres M R, Novoselov K S and Geim A K 2009 *Rev. Mod. Phys.* **81** 109
[34] Kotov V N, Uchoa B, Pereira V M, Guinea F and Castro Neto A H 2012 *Rev. Mod. Phys.* **84** 1067
[35] Cao Y, Fatemi V, Demir A, Fang S, Tomarken S L, Luo J Y, Sanchez-Yamagishi J D, Watanabe K, Taniguchi T, Kaxiras E, Ashoori R C and Jarillo-Herrero P 2018 *Nature* **556** 80
[36] Cao Y, Fatemi V, Fang S, Watanabe K, Taniguchi T, Kaxiras E and Jarillo-Herrero P 2018 *Nature* **556** 43
[37] Lopes dos Santos J M B, Peres N M R and Castro Neto A H 2007 *Phys. Rev. Lett.* **99** 256802
[38] Ahn S J, Moon P, Kim T H, Kim H W, Shin H C, Kim E H, Cha H W, Kahng S J, Kim P, Koshino M, Son Y W, Yang C W and Ahn J R 2018 *Science* **361** 782
[39] Yao W, Wang E, Bao C, Zhang Y, Zhang K, Bao K, Chan C K, Chen C, Avila J, Asensio M C, Zhu J and Zhou S 2018 *Proc. Natl. Acad. Sci. USA* **115** 6928
[40] Qiao Z, Tse W K, Jiang H, Yao Y and Niu Q 2011 *Phys. Rev. Lett.* **107** 256801
[41] Wang Z F, Liu F and Chou M Y 2012 *Nano Lett.* **12** 3833
[42] Loring T A and Hastings M B 2010 *Europhys. Lett.* **92** 67004
[43] Hastings M B and Loring T A 2011 *Ann. Phys.* **326** 1699
[44] Loring T A 2015 *Ann. Phys.* **356** 383
[45] Wang Z F and Liu F 2010 *ACS Nano* **4** 2459
[46] Qiao Z, Ren W, Chen H, Bellaiche L, Zhang Z, MacDonald A H and Niu Q 2014 *Phys. Rev. Lett.* **112** 116404